

A modeling study of the direct effect of aerosols over the tropical Indian Ocean

I. A. Podgorny and V. Ramanathan

Center for Atmospheric Sciences, Scripps Institution of Oceanography, University of California, San Diego, La Jolla, California, USA

Abstract. The microphysical, chemical, optical, and lidar data collected during the Indian Ocean Experiment (INDOEX) resulted in a self-consistent aerosol formulation for a multiple-scattering Monte Carlo radiation model. The model was used to simulate the direct aerosol radiative forcing, cloud radiative forcing, and heating rates for typical winter monsoon conditions over the tropical Indian Ocean. The focus of the study is to understand how the anthropogenic and natural aerosols partition the incoming solar energy between the ocean mixed layer and the overlying cloudy atmosphere. The observed aerosol single-scattering albedo, ω , was in the range 0.8–0.9 at 500 nm, mean aerosol visible optical thickness, τ_A , was in the range 0.1–0.8 at 500 nm, and the low-level clouds had horizontal scales of few kilometers and a cloud fraction of about 25%, typical of low-level clouds in the tropical oceans. The aerosol layer extended well above the low-level clouds in many instances, which has a significant impact on the radiative forcing. Although contributing only about 10% to the aerosol optical thickness, the soot transported from Asia and the Indian subcontinent significantly affects the aerosol direct forcing of the cloudy atmosphere. For monthly mean conditions ($\tau_A = 0.4$, $\omega = 0.9$ and 25% low-cloud fraction), the diurnal mean surface radiative forcing is about -25 W m^{-2} and the atmospheric forcing ranges from $+22$ to $+25 \text{ W m}^{-2}$. The top-of-the-atmosphere direct aerosol forcing is in the range of zero to -3 W m^{-2} . The aerosol enhances the cloud atmospheric forcing by 0.5 and by 2.5 W m^{-2} when aerosol is mostly below and above the clouds, respectively. Furthermore, the trade wind boundary layer is subject to a heating of about 1 to 1.5 K/d which might burn off the trade cumulus themselves. Thus the major impact of the predominantly anthropogenic aerosol over the tropical Indian Ocean is a substantial redistribution of the solar energy between the atmosphere and the ocean mixed layer.

1. Introduction

The Indian Ocean Experiment (INDOEX) was designed to study effects of air pollution on climate processes over the tropical Indian Ocean [Ramanathan *et al.*, 1996, 2001]. The pollutants, mainly in the form of aerosols, are produced over Asia and the Indian subcontinent and then transported to the Indian Ocean during the Northern Hemisphere winter monsoon. The INDOEX consisted of two field campaigns: the First Field Phase (FFP) in February–March 1998 and the Intensive Field Phase (IFP) in February–March 1999. One of the major goals of INDOEX was to document aerosol impact on solar radiation.

Satheesh *et al.* [1999] used aerosol chemical, microphysical, and optical and radiometric data collected at the island of Kaashidhoo (4.97°N , 73.47°E) during the INDOEX FFP to develop a comprehensive aerosol model for the natural and anthropogenic aerosols over the tropical Indian Ocean. The aerosol model was integrated with a multiple-scattering Monte Carlo radiative transfer model and calibrated at the surface with broadband flux measurements and at the top of the atmosphere (TOA) with the Clouds and Earth Radiant Energy System (CERES) radiation budget measurements. The agree-

ment between calculated and measured short-wave fluxes for both surface and TOA was within a few percent under clear skies [Satheesh *et al.*, 1999; Podgorny *et al.*, 2000]. It was found that the surface fluxes at local noon decreased by as much as 50 to 80 W m^{-2} and TOA fluxes increased by as much as 15 W m^{-2} during the INDOEX FFP as a consequence of aerosol pollution mostly of anthropogenic origin.

During the INDOEX IFP, the investigators used multiple aircraft, ships, and island stations over the Arabian Sea and the Indian Ocean [Ramanathan *et al.*, 1996, 2001]. One of the most striking observations during INDOEX was a dense brownish pollution haze layer, extending from the ocean surface up to almost 4000 m during the whole 6-week IFP (Plate 1). Low-level clouds were typically embedded in the aerosol layer. A large part of aerosol represented “dark” particles, such as soot, dust, and ash, so aerosol single scattering albedo measured at the ambient relative humidity, ω , occasionally dropped to values as low as 0.8 at 500 nm. The monthly mean aerosol optical thickness at 500 nm was as high as 0.4 with a daily range from 0.1 to 0.8 during the INDOEX IFP [Satheesh and Ramanathan, 2000; Ramanathan *et al.*, 2001]. The area affected by aerosol included most of the northern Indian Ocean, i.e., the Arabian Sea, much of the Bay of Bengal, and the equatorial Indian Ocean to about 5° south of the equator.

Several papers published within the last few years [Jayaraman *et al.*, 1998; Meywerk and Ramanathan, 1999; Podgorny *et al.*, 2000; Satheesh and Ramanathan, 2000] have documented

Copyright 2001 by the American Geophysical Union.

Paper number 2001JD900214.
0148-0227/01/2001JD900214\$09.00



Plate 1. An aircraft image of low-level clouds embedded in aerosol layer at the INDOEX site (February 1999).

the nature and magnitude of the direct aerosol radiative forcing in clear skies over the tropical Indian Ocean. Together, these papers reveal a substantial aerosol forcing at the surface and also show that the surface forcing is larger than that at the TOA by more than a factor of 3 under clear skies [Satheesh and Ramanathan, 2000]. The primary reason for this is the significant atmospheric absorption by the soot in the haze layer. The INDOEX results support recent observations and deductions from the TARFOX field study over the northern Atlantic Ocean just off the eastern U.S. seaboard [Hegg *et al.*, 1997; Novakov *et al.*, 1997; Russell *et al.*, 1999], and the SCAR-B field studies in Brazil [Kaufman *et al.*, 1998; Reid *et al.*, 1998], where low single-scattering albedos were measured. Ackerman and Toon [1981], Chylek *et al.* [1984], and Hansen *et al.* [1997] have also studied the importance of absorbing aerosols to climate.

The next important step is to extend the INDOEX studies to cloudy skies, which poses numerous obstacles. The presence of clouds can dramatically enhance the radiative impact of absorbing aerosols, particularly when aerosol is above the clouds [e.g., Haywood and Shine, 1997; Liao and Seinfeld, 1998]. The sign of the forcing may itself change depending on cloud amount, cloud albedo, and cloud spatial structure. The next difficulty is that the forcing magnitude (and possibly the sign) may strongly depend on aerosol vertical distribution. Recent field observations (TARFOX, SCAR-B, and INDOEX) have clearly revealed the hybrid structure of the vertical distribution. It ranges from a profile in which most of the aerosol is confined within the subcloud layer (1000–2000 m above the surface) to one in which the peak aerosol concentration is located at around 3000 m, well above the tops of low clouds. Such elevated aerosol layers have also been found in other tropical regions [e.g., Kaufman *et al.*, 1998]. Another formidable obstacle is the aerosol indirect forcing, in which the cloud properties over the northern Indian Ocean are themselves modified by the presence of aerosols [Ramanathan *et al.*, 2001].

When these issues are considered in conjunction with the uncertainties in radiometric and cloud observations, it is very difficult to quantify the aerosol forcing in cloudy regions directly from observations. What we need is an integrated approach that combines models with observations.

Toward this goal, the study employs a Monte Carlo cloud-aerosol-radiation interaction model. While the input of aerosol, cloud, and atmospheric properties to this model does not replicate any particular observation, it includes the range of values observed in the INDOEX region from surface, aircraft, and satellites. In particular, we consider two distinctive aerosol vertical distributions identified during INDOEX and use low-level clouds as an input to the radiative transfer model. Our objective is to elucidate the sign, magnitude, and vertical structure of the aerosol forcing. The consideration is limited to the aerosol effect on solar fluxes, since the aerosol effect on thermal radiation over the northern Indian Ocean is minor [Lubin *et al.*, 2001].

The main focus of this study is the direct aerosol forcing over the northern Indian Ocean during the winter monsoon period. We adopt a broad definition of aerosol radiative forcing following Satheesh *et al.* [1999]. Specifically, it is defined as the effect of aerosol, both natural and anthropogenic, on the net short-wave radiative fluxes at the TOA and surface and on the absorption of short-wave radiation in the atmosphere. In such a way, we have three types of aerosol forcing, i.e., TOA radiative forcing R_T , surface radiative forcing R_S , and atmospheric radiative forcing R_A . The three types of forcing are constrained by the following equation:

$$R_T = R_S + R_A. \quad (1)$$

R_T usually receives most attention because it determines the effect of aerosol on the net solar energy input to the climate system [e.g., Charlson *et al.*, 1992; Kiehl and Briegleb, 1993; Haywood *et al.*, 1997]. Although the R_T value can be nearly

zero for the absorbing aerosol [e.g., Hansen *et al.*, 1997], the absolute values of R_S and R_A can be large due to redistribution of solar energy in the atmosphere-ocean system by the aerosol. Since the ocean surface albedo is low, the aerosol increases the solar energy absorption in the atmosphere at the expense of the solar energy deposited in the ocean. The excess solar absorption in the atmosphere due to absorbing aerosol (positive R_A and negative R_S) can change the net equator-to-pole heating gradient of atmosphere and oceans, the hydrological cycle, and the surface heat budget. Thus perturbation of the climate system due to the relatively large R_A can be more important than perturbation due to the relatively small R_T . Finally, we need to quantify the aerosol modulation of heating rates in the atmosphere in order to better understand the effect of aerosol-induced absorption on cloud dynamics.

2. Description of the Model

2.1. Aerosol Model

The aerosol model used in this study is based on aerosol chemical, microphysical, and optical and radiometric data collected during the INDOEX FFP and described in detail by Sathesh *et al.* [1999]. The directly measured aerosol species include sea salt, dust, and sulfate. The inferred species include soot, organics, and ash. The aerosol species contribute to the aerosol optical thickness at 500 nm in the following way: sea salt, 17%; mineral dust, 15%; sulfate and ammonium, 29%; soot, 11%; organics, 20%; and fly ash, 8% (see Sathesh *et al.* [1999] for more detail). The soot component is used following the definition by Hess *et al.* [1998] to represent absorbing black carbon. The aerosol model was calibrated using the surface radiometric observations at the island of Kaashidhoo and the CERES radiation measurements [Sathesh *et al.*, 1999; Podgorny *et al.*, 2000]. The calculated surface fluxes under clear skies agreed with the measurements within a few W m^{-2} , which is less than the instrumental error. Furthermore, the calculated aerosol-scattering coefficients were within the range of measured values typical for oceanic regions [Sathesh *et al.*, 1999].

The first aerosol vertical distribution used as input to the model is derived from scanning aerosol back scatter lidar measurements from R/V *Sagar Kanya* in the vicinity of Kaashidhoo during the INDOEX FFP [Sathesh *et al.*, 1999]. The distribution is uniform in the boundary layer (up to 1000 m) and then exponentially decreasing with a scale height of 800 m (Figure 1, top). The aerosol forcing calculations reported by Sathesh *et al.* [1999] and Podgorny *et al.* [2000] are based on this type of vertical distribution.

A heavy elevated aerosol layer was frequently observed from aircraft to the north of Kaashidhoo during the INDOEX IFP [Ramanathan *et al.*, 2001]. The corresponding aerosol profile is peaked between 3000 and 3500 m, the magnitude of aerosol extinction coefficient being 3 times larger than that in the boundary layer (Figure 1, top). On the basis of the INDOEX IFP and FFP observations, we postulate that instantaneous aerosol vertical distributions in the tropical Indian Ocean during winter monsoon fall between the two profiles presented in Figure 1. The aerosol vertical distributions are assumed the same for all aerosol species. Here $\tau = 0.9$ at 500 nm was typically observed during the INDOEX for both types of aerosol vertical distribution [Ramanathan *et al.*, 2001] and is used for most calculations. We also perform numerical experiments with the model in which τ varies from 0.8 to 1.0 in order to

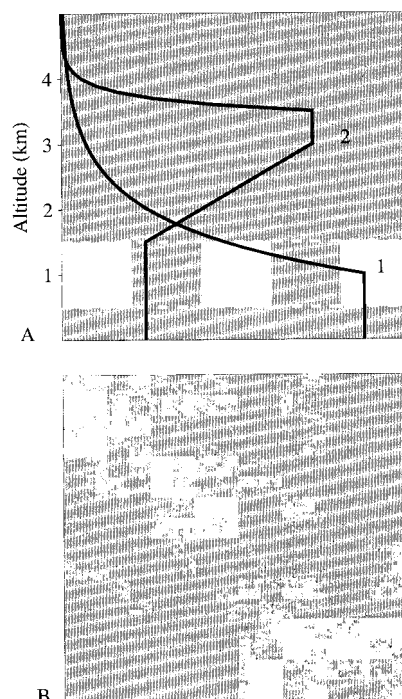


Figure 1. Side view of cloud and aerosol vertical profiles with aerosol mostly (1) below and (2) above cloud tops (a). Top view of a fractal cloud scene (b). Clouds and ocean are shown in white and gray, respectively. The aerosol vertical profiles are to be multiplied by a given aerosol optical thickness to calculate aerosol extinction coefficient as a function of altitude.

investigate the effect of τ on aerosol radiative forcing. In this case, the soot content is adjusted in order to achieve the required τ values in the range 0.8–0.95. All aerosol species except for sea salt are replaced by sulfate and ammonium in order to model the limit case of conservatively scattering aerosol ($\tau = 1.0$). We use the average aerosol optical thickness of 0.4 (at 500 nm) observed during INDOEX IFP [Sathesh and Ramanathan, 2000] for most numerical experiments.

Aerosol particles are assumed spherical, Mie phase function and single-scattering albedo for each aerosol species is computed using the OPAC 3.1 software [Hess *et al.*, 1998]. The model assumes aerosol species to be externally mixed. Pilinis *et al.* [1995] reported a negligible effect of mixing state on the aerosol forcing for a “global mean” aerosol model (sulfate, nitrate, sea salt, organic carbon, and crust material), although the model did not contain strongly absorbing aerosol. The sensitivity of the aerosol forcing to the mixing state is generally higher when a mixture of only soot and sulfate is considered [e.g., Haywood *et al.*, 1997, and references therein]. In particular, configuring the soot as a shell surrounding the aerosol particles would enhance the solar absorption significantly, but such particles cannot be justified as yet from observations. For the INDOEX aerosol model, the global fluxes at the surface under clear skies were calculated for both externally and internally mixed aerosol and agreed within 0.5% [Sathesh *et al.*, 1999; Podgorny *et al.*, 2000].

2.2. Radiative Transfer Model

The radiative transfer model used in this study is a three-dimensional (3-D) broadband Monte Carlo model developed at the Center for Clouds, Chemistry, and Climate (C4), Scripps

Institution of Oceanography [Podgorny *et al.*, 2000; Vogelmann *et al.*, 2001, and references therein]. The model accounts for all multiple scattering and absorption by individual aerosol species, cloud droplets, air molecules, and reflections from the surface. In the case of externally mixed aerosol, the probability of a scattering interaction with a particular aerosol species is determined by relative contribution of the species to the total aerosol extinction coefficient in a layer [Satheesh *et al.*, 1999; Podgorny *et al.*, 2000]. Scattering angles are computed by linear interpolation in a table of the inverse cumulative scattering probability [Barkstrom, 1995], so the model assimilates the Mie phase functions without compromising angular resolution.

Correlated k -distributions [Lacis and Oinas, 1991] are used to incorporate gaseous absorption by water vapor, ozone, oxygen, and carbon dioxide. The water vapor is saturated where the clouds are present. The model uses 25 bands and a total of 3132 pseudomonochromatic calculations to cover the solar spectrum from 0.25 to 5.0 μm (see Vogelmann *et al.* [2001] for more detail). The ocean surface albedo is calculated according to Briegleb *et al.* [1986] (see Podgorny *et al.* [2000] for more detail). The diurnal time averaging is performed by Monte Carlo integration over the solar zenith angle. In such a way, time expenses for calculating a broadband and diurnal average broadband fluxes are nearly the same.

2.3. Cloud Model

The cloud model is constrained by the following measurements during the INDOEX IFP: (1) cloud microphysical data (NCAR C-130 aircraft), (2) cloud base height (micropulse lidar), (3) low-level cloud fraction (Meteosat 5, ISCCP).

Aircraft observations of cloud drop effective radius, r , and cloud drop concentration, N , are used to estimate cloud extinction coefficient in the visible, k [Heymsfield and McFarquhar, 2001; Ramanathan *et al.*, 2001, and references therein]. As cloud drop effective radius exceeds wavelength in the visible by an order of magnitude, and hence the extinction efficiency is approximately 2, we have

$$k = 2\pi r^2 N. \quad (2)$$

Figure 2 shows k in the visible versus latitude for 1385 cloud passes in the 500–1500 m altitude range. The k values tend to cluster between zero and 50 km^{-1} ; the mean k value is 40 km^{-1} . Given that (1) typical cloud geometrical thickness for low-level clouds is about 500 m and (2) liquid water content measured by aircraft in the central parts of clouds is slightly higher than the average, the optical thickness of an individual cloud, τ_0 , is approximated by the value of 15 at 500 nm and then adjusted at each spectral band as described by Vogelmann *et al.* [2001]. This value represents an upper bound on the optical thickness of low-level clouds in the INDOEX region and is in a good agreement with the τ_0 value estimated by Ramanathan *et al.* [2001]. On the basis of INDOEX observations, Ramanathan *et al.* [2001] developed a composite scheme to relate aerosol optical thickness and cloud optical thickness for low-level clouds. In this scheme, the τ_0 value approaches 13.75 when optical thickness of aerosol exceeds 0.4.

An accurate modeling of aerosol-cloud radiative interactions would generally require a 3-D treatment of both aerosol and cloud spatial distributions. Whereas the C4 Monte Carlo radiative transfer model is capable of assimilating 3-D aerosol distributions, we resort to a simplified plane-parallel treatment of aerosol due to the lack of a proper 3-D model. Although the

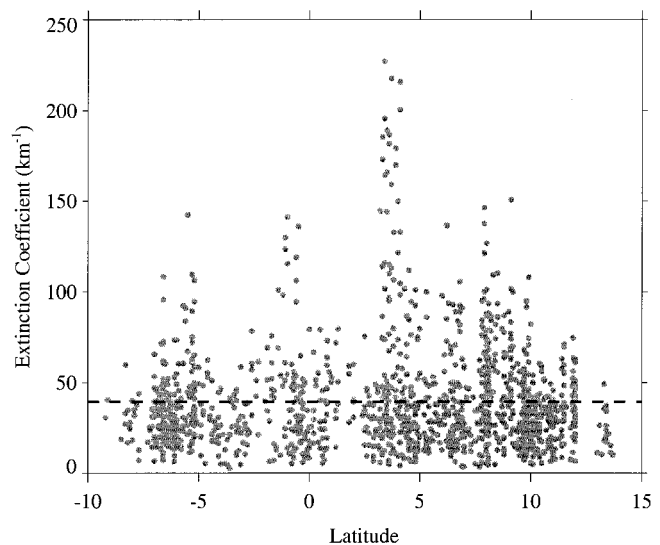


Figure 2. Low-level cloud extinction coefficient in the visible estimated from the NCAR C-130 aircraft observations during the INDOEX IFP. Dashed line shows the mean extinction coefficient.

use of 3-D aerosol distributions might alter aerosol forcing calculations under cloudy skies, the development of a 3-D cloud-aerosol model is beyond the scope of this paper.

When selecting an appropriate 3-D cloud model, we need first of all to account for the effects of cloud gaps and cloud-to-cloud radiative interactions as contributing most to the 3-D cloud effect on solar energy absorption for the case of low clouds [e.g., Podgorny *et al.*, 1998]. In such a way the cloud model would allow radiation to penetrate below the clouds through the gaps and reach the aerosol beneath the clouds. As the model neglects internal inhomogeneity in liquid water distribution and cloud top variations within an individual cloud, we refer hereinafter to the effects of cloud gaps and cloud-to-cloud radiative interactions as 3-D cloud effects. The synthetic cloud scenes are constructed following Marshak *et al.* [1998]. A stratiform cloud is first generated using a “bounded cascade” three-parameter fractal model [see Marshak *et al.*, 1998, for references] and then supplemented with gaps. To do that, a constant b is subtracted from the cloud optical thickness τ , the “negative” ($(\tau - b) < 0$) pixels are considered clear skies, and “positive” ($(\tau - b) > 0$) pixels are assigned a predetermined cloud optical thickness τ_0 . The b value is a function of “bounded cascade” model parameters and a given cloud fraction. A cloud scene has 256×256 pixels with a pixel size of 100 m (Figure 1, bottom).

During INDOEX, low-level cloud base altitudes in the northern Indian Ocean were between 500 and 1000 m and cloud top altitudes between 1000 and 1500 m (A. Heymsfield and G. McFarquhar, unpublished data, 1999, based on micropulse lidar observations during INDOEX FFP and IFP). We assign the cloud base altitude to be 500 m and use a uniform cloud extinction coefficient between 500 and 1500 m in each cloud pixel (Figure 1, top).

Figure 3 is the monthly mean low-level cloud fraction in the INDOEX region (55° – 75°E) versus latitude for the January–March period. The cloud fraction is calculated on the basis of two independent sources of cloud data: ISCCP [Rossow *et al.*, 1996] infrared low-level cloud fraction for 1989–1993 and

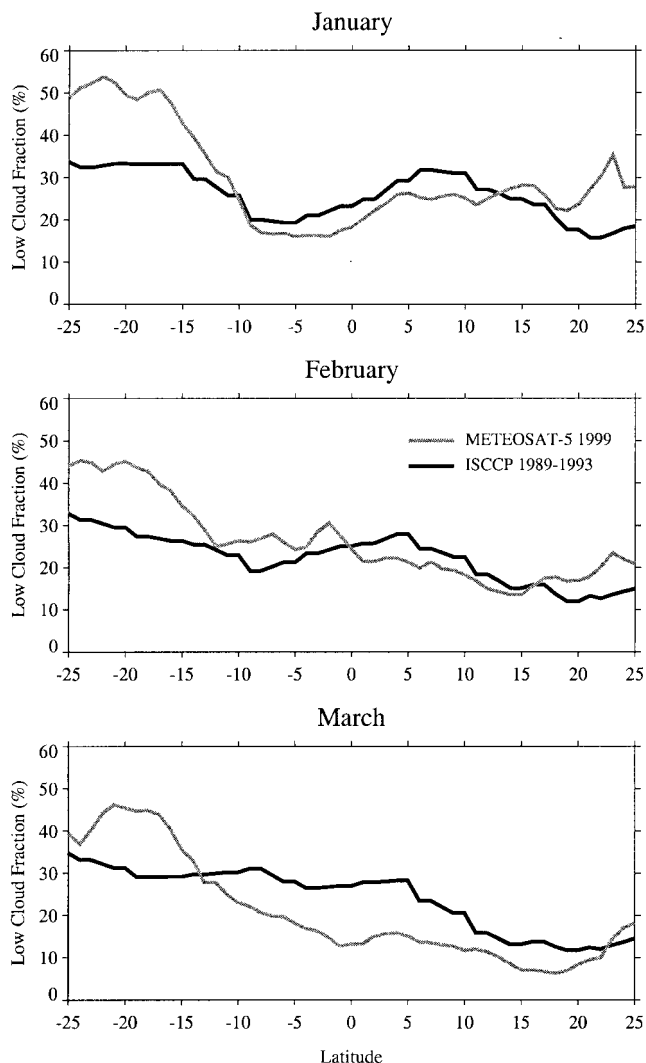


Figure 3. Monthly mean low-level cloud fraction in the INDOEX region (55° – 75° E) versus latitude for the January–March period.

Meteosat 5 low cloud fraction for 1999. Only nonoverlapped low-level clouds are reported in Figure 3. For February and March the monthly mean low-level cloud fraction gradually increases from 10–15% over the Arabian Sea to 30–50% over the Intertropical Convergence Zone (ITCZ). We adopt the 25% low-level cloud fraction as a representative value for the northern Indian Ocean during the INDOEX. The consideration is limited to the case of nonoverlapped low-level clouds for the following reasons: (1) low-level clouds were prevalent during INDOEX as supported by aircraft observations and satellite analysis [Ramanathan *et al.*, 2001]; (2) information on low-level clouds overlapped by high-level and midlevel clouds is not available from satellite observations; (3) effect of midlevel and high-level clouds on the aerosol forcing is limited in magnitude [e.g., Liao and Seinfeld, 1998].

3. Results

3.1. Magnitude of Aerosol Forcing

We first focus on the magnitude of aerosol radiative forcing as a function of cloud fraction, aerosol single-scattering albedo

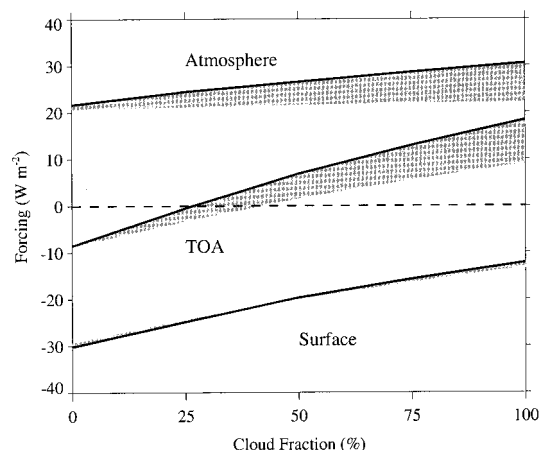


Figure 4. TOA, atmospheric, and surface direct radiative forcing as a function of cloud fraction. Aerosol optical thickness is 0.4, aerosol single-scattering albedo is 0.9, and cloud optical thickness is 15. Solid black line and the other edge of the gray region represent the cases with aerosol above and below clouds (see Figure 1), respectively.

and aerosol vertical distribution. The results of calculations are presented for diurnal average aerosol radiative forcing defined as an average forcing during the 24-hour period. As the aerosol below and above the clouds is thought to represent two extreme cases with respect to aerosol forcing, the area between the two curves is shaded to display the forcing for a variety of instantaneous aerosol vertical distributions.

Figure 4 (top) shows the TOA, atmospheric and surface direct aerosol radiative forcing versus cloud fraction for $\tau = 0.9$. As seen from Figure 4, R_S is only a function of the cloud fraction, nearly insensitive to the aerosol vertical distribution and always negative. On the contrary, R_A is almost independent of cloud fraction for the aerosol below clouds and increases by less than 5 W m^{-2} when the aerosol is above the clouds. The effect of aerosol vertical distribution on R_A is negligible under clear skies, increasing with cloud fraction and reaching the maximum under overcast skies. R_T depends on both cloud fraction and aerosol vertical distribution in the most complicated way. The difference between two vertical aerosol distributions has virtually no effect on the TOA forcing under clear skies but reaches the maximum under overcast. In absolute values the TOA forcing under overcast skies is twice as large when aerosol is mostly above the clouds. This is hardly surprising, however, given that the overcast clouds have the strongest reflection. In such a way, absorbing aerosols above and in the upper part of clouds contribute most in reducing the upward radiative flux at the TOA. R_T is negative under clear skies but becomes positive when the cloud fraction is about 25 and 40% for the aerosol mostly above and below the clouds, respectively.

In plane-parallel approximation (e.g., assuming that the pixel size is orders of magnitude larger than cloud geometrical thickness) the relationship between aerosol forcing and cloud fraction is a straight line connecting two extreme cases of the forcing under clear and overcast skies. As seen from Figure 4, the 3-D cloud effect increases the TOA forcing by ~ 1 – 2 W m^{-2} when cloud fraction is between 25 and 50%; that is, 3-D radiation-cloud interactions tend to decrease the reflection of solar radiation by aerosols back to space. The effects of internal inhomogeneity in liquid water distribution within an indi-

Table 1. TOA (R_T), Atmospheric (R_A), and Surface (R_S) Radiative Forcing (W m^{-2}) Under Cloudy Skies As a Function of Cloud Fraction (f) and Aerosol Optical Thickness (τ_A)^a

	f , %	τ_A	R_T	R_A	R_S
Arabian Sea	15	0.8	-6.3	44.1	-50.4
Maldives	25	0.4	-0.8	24.0	-24.8
ITCZ	50	0.1	1.7	6.9	-5.2

^aCloud optical thickness is 15.

vidual cloud might decrease the positive TOA forcing by about 15% in the limiting case of overcast clouds [Highwood, 2000].

We now focus on sensitivity of aerosol forcing to the cloud top altitude and compute R_T for a cloud field confined between 500 and 1000 m (cloud fraction is 25% and cloud optical thickness is 15). When cloud top altitude decreases from 1500 to 1000 m, the positive contribution of absorbing aerosol to the TOA forcing raises reflecting additional absorption by extra aerosol above the cloud tops. The magnitude of this increase is relatively small, being 0.9 and 0.1 W m^{-2} for the aerosol mostly above and below the clouds, respectively.

As both cloud fraction (Figure 3) and aerosol optical thickness [Jayaraman *et al.*, 1998; Ramanathan *et al.*, 2001] vary across the northern Indian Ocean, the aerosol forcing should be a function of latitude. To address this issue in more detail, Table 1 shows aerosol forcing calculated for three representative regions: Arabian Sea (large aerosol optical thickness, small cloud fraction), Maldives (aerosol and cloud parameters used throughout this study to represent average INDOEX conditions), and ITCZ (small aerosol optical thickness and large cloud fraction). The aerosol forcing is computed for a combination of the first (weighted by a factor of 1/3) and second (weighted by a factor of 2/3) aerosol profiles (see Figure 1), as the boundary layer aerosol profile occurred about one third of the time and the elevated profile about two thirds of the time during the INDOEX IFP [Ramanathan *et al.*, 2001]. As seen from Table 1, the magnitude of the forcing decreases southward, following the latitudinal trend in aerosol optical thickness. The increase in cloud fraction from Arabian Sea to ITCZ changes the sign of the TOA forcing.

We next investigate the effect of aerosol single-scattering albedo on the aerosol forcing. Figure 5 shows the direct aerosol radiative forcing versus ω . Calculations are made for cloudy skies (25% cloud fraction), both aerosol vertical distributions (corresponding to the boundaries of the shaded area), and for clear skies (solid line). R_T is positive when ω drops below 0.9 and 0.83 for the aerosol above and below the clouds, respectively. The effect of clouds on the atmospheric forcing is minor when aerosol is below clouds even for the relatively low ω values. When aerosol is above the clouds, the cloud contribution to R_A is about 15–20% for the typical ω values over the tropical Indian Ocean. The presence of clouds diminishes the surface forcing for all considered ω .

3.2. Aerosol Effect on Cloud Forcing

The TOA cloud radiative forcing, C_T , is defined as the difference between net short-wave fluxes at the TOA for cloudy and clear-sky atmosphere [e.g., Ramanathan *et al.*, 1995]. The TOA forcing is generally negative since clouds tend to reflect more solar radiation back to space than a cloudless atmosphere. Similarly, the surface cloud forcing, C_S , or the

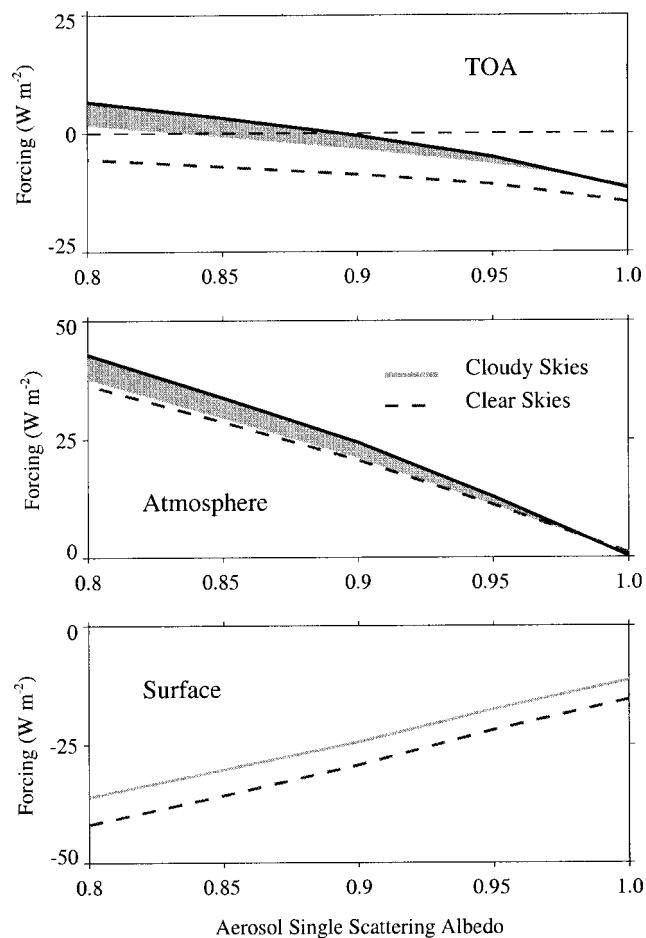


Figure 5. TOA (top), atmospheric (middle), and surface (bottom), radiative forcing for clear (solid line) and cloudy (shaded area) skies as a function of aerosol single-scattering albedo. Aerosol optical thickness is 0.4, cloud fraction is 25%, and cloud optical thickness is 15. Solid black line and the other edge of the gray region represent the cases with aerosol above and below cloud (see Figure 1), respectively.

difference between cloudy and clear-sky net short-wave fluxes at the surface is negative, as the clouds prevent solar radiation from reaching the surface. Finally, the atmospheric cloud forcing, C_A , is the difference between bulk atmospheric absorption in the cloudy and cloudless atmosphere. The three types of the cloud forcing are constrained by the following equation:

$$C_T = C_S + C_A. \quad (3)$$

The cloud forcing is zero under clear skies increasing in magnitude with cloud fraction.

Figure 6 shows the cloud forcing versus cloud fraction calculated for a pristine (dashed line) and polluted (shaded regions) atmosphere. For the 25% cloud fraction, the aerosol-free atmospheric cloud forcing is 7.0 W m^{-2} . The presence of aerosol ($\omega = 0.9$) results in a stronger cloud forcing with magnitude ranging from 7.5 W m^{-2} (aerosol mostly below the clouds) to 10.0 W m^{-2} (aerosol mostly above the clouds).

Ramanathan *et al.* [1995] used the ratio $f_S = C_S/C_T$ to quantify the effect of clouds on atmospheric absorption. According to (3) the atmospheric cloud forcing is positive when the surface forcing exceeds the TOA cloud forcing in magnitude; that is, $f_S > 1$. On the basis of the results shown in

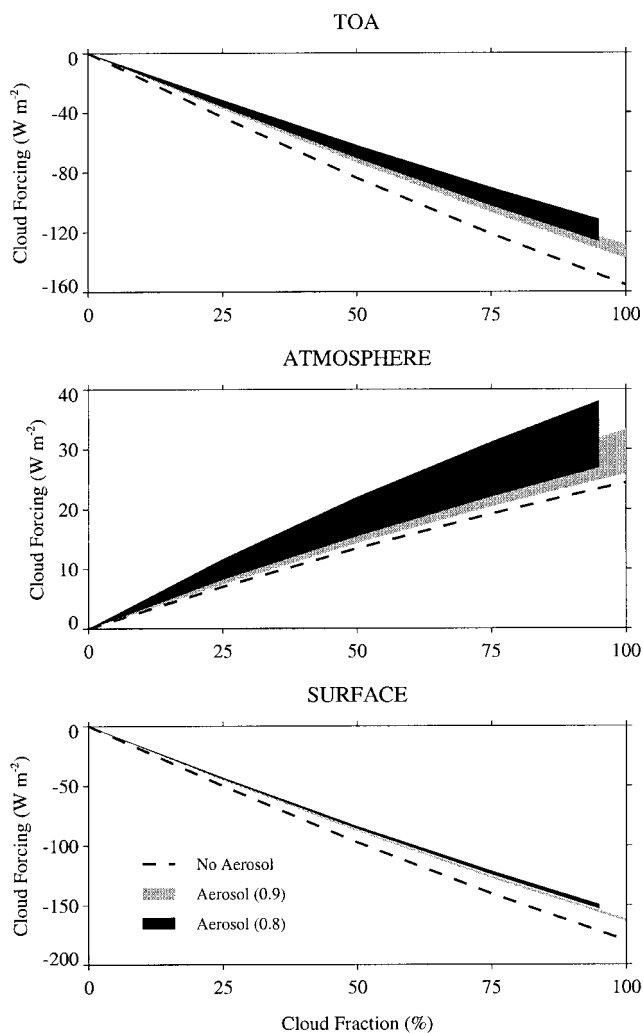


Figure 6. Cloud radiative forcing versus cloud fraction in a pristine (dashed line) and polluted (shaded regions) atmosphere. The bounding lines of gray ($\tau = 0.9$) and black ($\tau = 0.8$) regions represent the cases with aerosol above and below cloud (see Figure 1). Aerosol optical thickness is 0.4.

Figure 6, the f_s value is 1.16 in a pristine atmosphere, 1.20 when aerosol is below the clouds and $\tau = 0.9$, and 1.37 when aerosol is above the clouds and $\tau = 0.8$.

3.3. Aerosol Modulation of Diurnal Mean Heating Rates in the Atmosphere

In this section we focus on the heating rates in the lower (below 5000 m) troposphere. Figure 7 (left) shows the heating rates in a pristine atmosphere. Calculations are made under clear skies (solid line) and cloudy atmosphere (dashed line) with a cloud fraction of 25%. Both curves are nearly the same above 1500 m (cloud top altitude). In the 500–1500 m layer, heating rates in the cloudy atmosphere exceed those under clear skies by a factor of 2. Figure 7 (right) shows the enhancement in the heating rates by aerosols for two τ values: 0.9 (gray) and 0.8 (black). A distinction is now made between two aerosol vertical distributions. Aerosols nearly double the heating rates both for clear and for cloudy skies with the largest increase in heating rates observed in the layer of maximum aerosol concentration above the clouds.

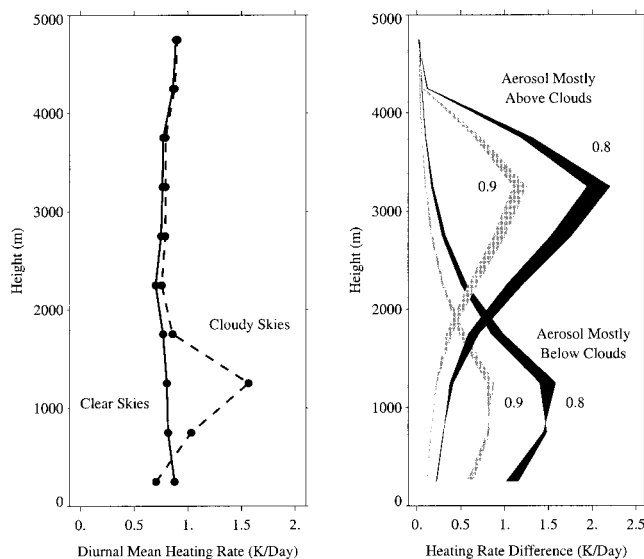


Figure 7. Heating rates in a pristine atmosphere (left) and aerosol contributions to heating rates (right). Aerosol single-scattering albedo is 0.8 (black region) and 0.9 (gray region), aerosol optical thickness is 0.4, cloud fraction is 25%, and cloud optical thickness is 15. The bounding lines of shaded regions represent clear and cloudy skies.

3.4. Role of Soot and Dust in the Aerosol Forcing

As mentioned in section 3.1, we assume that aerosol is externally mixed. While this assumption has a minor effect on the magnitude of the aerosol forcing [Satheesh *et al.*, 1999; Podgorny *et al.*, 2000], it allows us to estimate contributions from individual aerosol species to the direct aerosol forcing. These are computed by repeating the radiative transfer calculations for each species while assigning all other species concentrations to be zero. In such a way, the optical thickness for each per species calculation is limited to the optical thickness contributed by that species. Because of nonlinearity of the optical effects, the per species forcings do not necessarily add up to the forcing for the mixture of aerosol, although this effect is negligible. Figure 8 displays the contributions from soot (black), dust (gray), and other species (white) in the form of bar charts. The optical thickness for the sum of all the aerosols is 0.4 at 500 nm, cloud fraction is 25%, and cloud optical thickness is 15 for all cases.

As seen from Figure 8 (top), the soot contribution to the TOA forcing is small but positive in cloudless atmosphere. Because of extremely low single-scattering albedo (0.23 at 500 nm; see Satheesh *et al.* [1999]), soot strongly absorbs radiation reflected upward from the lower layers of the atmosphere (Rayleigh scattering) and the ocean surface. The effects of soot and dust on the TOA forcing increase dramatically under cloudy skies, as the soot becomes the leading contributor to the TOA forcing for the case of aerosol above the clouds. The contribution from other species decreases in magnitude as those species (e.g., ash) also absorb the solar radiation reflected by the clouds. The positive contribution from soot and dust virtually cancels negative contributions from sea salt and sulfate, so the TOA forcing is negligible under cloudy skies (see Figure 4). The soot and dust contributions are larger when aerosol is mostly above the clouds as the soot and dust act more efficiently, absorbing the solar radiation both on the way down to the clouds and on the way up after reflection from the

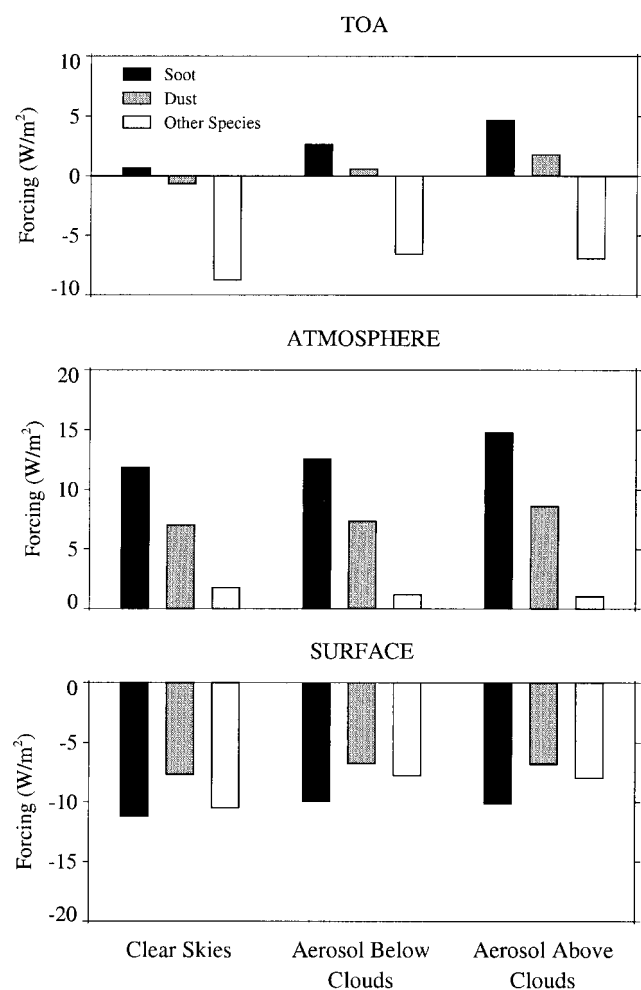


Figure 8. Contribution of aerosol species to the aerosol radiative forcing. Aerosol single-scattering albedo is 0.9, aerosol optical thickness is 0.4 for the sum of all the aerosols, cloud fraction is 25%, and cloud optical thickness is 15. (a) Clear skies, (b) cloudy skies, aerosol mostly below the clouds. (c) Cloudy skies, aerosol mostly above the clouds.

clouds. The relatively large effect of clouds on the TOA forcing is a consequence of the low surface albedo, so the appearance of low clouds alters reflection from beneath the absorbing aerosol significantly.

Soot (57%) and dust (34%) dominate the atmospheric forcing under clear skies (Figure 8, middle), which means that the soot is the major contributor to the anthropogenic effects on the atmospheric aerosol forcing. The relative soot and dust contributions to the atmospheric forcing are nearly the same under the cloudy and clear skies. The type of vertical aerosol distribution affects the magnitude of the atmospheric forcing but does not the relative species contributions.

Finally, soot and dust are the most significant contributors to the aerosol forcing at the surface (Figure 8, bottom) too. Contributions from other species to the surface forcing are caused by both absorption of direct radiation by aerosol (e.g., dust) and scattering of radiation upward (e.g., sulfate and ammonium).

4. Conclusion

The tropics in general, and the tropical Indian Ocean in particular, have a complex structure of 3-D low-level clouds. It

is a formidable challenge to unravel the direct and indirect effect of aerosols in such cloudy regions solely from radiation observations. This modeling study provides estimates for the direct forcing. Since the model employs observations of aerosol and cloud microphysical properties as input for the radiative computations, the aerosol forcing results shown here should provide a sound framework for analyzing the impact of absorbing aerosol over the northern Indian Ocean on the climate system.

The main conclusion emerging from the results presented in this paper is that the direct effect of the aerosol in the cloudy atmosphere is a large reduction in the solar energy absorbed by the surface (-25 W m^{-2}) and a correspondingly large increase in the lower atmospheric solar heating. The TOA direct forcing has a hybrid structure, switching from a negative forcing under clear skies to a positive forcing under overcast conditions. However, when the indirect effect of on cloud optical depth is included, the total aerosol forcing can be moderately negative [Ramanathan *et al.*, 2001].

The large negative forcing at the surface has significant implications to the hydrological cycle. For the tropics as a whole, roughly 80% of the annual mean net radiative heating at the surface is balanced by evaporation [Oberhuber, 1988]. Thus the decline in surface solar heating can result in a reduced evaporation. The aerosol-induced doubling of the solar heating of the lower troposphere (see Figure 7) can also turn off the trade cumulus clouds since these clouds are sensitive to solar absorption [Ackerman *et al.*, 2000]. The fundamental implication is that we need to focus on how the absorbing aerosols perturb the hydrological cycle instead of dismissing their climatic effect because of the relatively small magnitude of TOA forcing over the northern Indian Ocean. The primary reason for the large surface forcing and small TOA forcing is the absorption of solar radiation by the aerosol that is discussed next.

One of the goals of this study is to investigate the role of soot in the aerosol radiative forcing over the northern Indian Ocean. Soot is the most important aerosol species of anthropogenic origin with respect to the aerosol radiative forcing, as a relatively small variation in soot content can produce a dramatic change in the aerosol single-scattering albedo. Removing the soot from the aerosol model used in this study would result in the ω value as high as 0.96, compared to $\omega = 0.8-0.9$ observed during the INDOEX IFP. As previously found by Hegg *et al.* [1997] and Novakov *et al.* [1997] for the U.S. eastern seaboard, we demonstrated that soot is the largest contributor to the atmospheric forcing over the northern Indian Ocean in both cloudy and cloudless atmosphere and the major contributor to the TOA forcing under cloudy skies. The relative contributions of soot and dust to the aerosol forcing increase with cloud fraction. The location of an aerosol layer with respect to the cloud top strongly affects the soot contribution to the TOA forcing. It increases almost twofold, from 2.7 to 4.7 W m^{-2} , when the aerosol is above compared to the aerosol mostly below the clouds. On the contrary, the vertical distribution of aerosol plays a minor role in the aerosol radiative forcing under clear skies. The presence of aerosol ($\omega = 0.9$) increases cloud forcing by 0.5 and by 2.5 W m^{-2} for the cases of aerosol mostly below and above the clouds, respectively. The associated increase in the ratio of the surface to the TOA cloud forcing is consistent with an increased atmospheric absorption due to the presence of absorbing aerosol. Cloud-to-cloud radiative interactions tend to increase atmospheric absorption by

the absorbing aerosol at the expense of the solar radiation reflected back to space, but this effect is insignificant.

Although the accurate estimation of the aerosol TOA forcing over the tropical Indian Ocean represents a complex problem and needs further analysis of the INDOEX data, the relative effect of the TOA forcing on the local climate system seems to be minor. On the contrary, the impact of absorbing aerosol on the redistribution of solar energy in the atmosphere-ocean system is tremendous, with up to the 30% decrease in the solar energy absorbed by the ocean. Furthermore, the aerosol contributions to the heating rates in the lower troposphere can be as large as the heating rates in a pristine atmosphere. Numerical experiments with GCMs would be helpful in estimating the consequences of aerosol-induced ocean-atmosphere redistribution of the solar energy on the tropical Indian Ocean climate.

Acknowledgments. This work was supported by the NSF Science and Technology Center for Clouds, Chemistry and Climate (C4), and this is C4 publication 217 and INDOEX publication 59. We thank D. Baumgardner, G. McFarquhar, and S. K. Satheesh for the permission to use the INDOEX IFP unpublished data as input for the model, S. Rupert for Meteosat 5 analysis used in Figure 3, A. Vogelmann for assistance with the broadband Monte Carlo calculations, and anonymous reviewers for valuable comments on the manuscript.

References

- Ackerman, S., and O. B. Toon, Absorption of visible radiation in atmosphere containing mixtures of absorbing and nonabsorbing particles, *Appl. Opt.*, **20**, 3661–3668, 1981.
- Ackerman, A. S., O. B. Toon, D. E. Stevens, A. J. Heymsfield, V. Ramanathan, and E. J. Welton, Reduction of tropical cloudiness by soot, *Science*, **288**, 1042–1047, 2000.
- Barkstrom, B., An efficient algorithm for choosing scattering direction in Monte Carlo work with arbitrary phase functions, *J. Quant. Spectrosc. Radiat. Transfer*, **53**, 23–38, 1995.
- Briegleb, B. P., P. Minnis, V. Ramanathan, and E. Harrison, Comparison of regional clear-sky albedos inferred from observations and model computations, *J. Clim. Appl. Meteorol.*, **25**, 214–226, 1986.
- Charlson, R. J., S. E. Schwartz, J. M. Hales, R. D. Cess, J. A. Coakley, J. E. Hansen, and D. J. Hofmann, Climate forcing by atmospheric aerosols, *Science*, **255**, 423–430, 1992.
- Chylek, P., V. Ramaswamy, and R. J. Cheng, Effect of graphitic carbon on the albedo of clouds, *J. Atmos. Sci.*, **41**, 3076–3084, 1984.
- Hansen, J., M. Sato, and R. Ruedy, Radiative forcing and climate response, *J. Geophys. Res.*, **102**, 6831–6864, 1997.
- Haywood, J. M., and K. P. Shine, Multispectral calculations of the direct radiative forcing of tropospheric sulfate and soot aerosols using a column model, *Q. J. R. Meteorol. Soc.*, **123**, 1907–1930, 1997.
- Haywood, J. M., D. L. Roberts, A. Slingo, J. M. Edwards, and K. P. Shine, General circulation model calculations of the direct radiative forcing by anthropogenic sulfate and fossil-fuel soot aerosol, *J. Clim.*, **10**, 1562–1577, 1997.
- Hegg, D. A., J. Livingston, P. V. Hobbs, T. Novakov, and P. Russell, Chemical apportionment of aerosol column optical depth off the mid-Atlantic coast of the United States, *J. Geophys. Res.*, **102**, 25,293–25,303, 1997.
- Hess, M., P. Koepke, and I. Schult, Optical properties of aerosols and clouds: The software package OPAC, *Bull. Am. Meteorol. Soc.*, **79**, 831–844, 1998.
- Heymsfield, A. J., and G. M. McFarquhar, Microphysics of INDOEX clean and polluted clouds, *J. Geophys. Res.*, in press, 2001.
- Highwood, E. J., Effect of cloud inhomogeneity on direct radiative forcing due to aerosols, *J. Geophys. Res.*, **105**, 17,843–17,852, 2000.
- Jayaraman, A., A. D. Lubin, S. Ramachandran, V. Ramanathan, E. Woodbridge, W. Collins, and K. S. Zalpuri, Direct observations of aerosol radiative forcing over the tropical Indian Ocean during the January–February 1996 pre-INDOEX cruise, *J. Geophys. Res.*, **103**, 13,827–13,836, 1998.
- Kaufmann, Y. J., et al., Smoke, Clouds, and Radiation–Brazil (SCAR–B) experiment, *J. Geophys. Res.*, **103**, 31,783–31,808, 1998.
- Kiehl, J. T., and B. P. Briegleb, The relative roles of sulfate aerosol and greenhouse gases in climate forcing, *Science*, **260**, 311–314, 1993.
- Lacis, A. A., and V. Oinas, A description of the correlated *k* distribution method for modeling nongray gaseous absorption, thermal emission, and multiple scattering in vertically inhomogeneous atmospheres, *J. Geophys. Res.*, **96**, 9027–9063, 1991.
- Liao, H., and J. H. Seinfeld, Effect of clouds on direct aerosol radiative forcing of climate, *J. Geophys. Res.*, **103**, 3781–3788, 1998.
- Lubin, D., S. K. Satheesh, A. Heymsfield, and G. McFarquhar, The longwave radiative forcing of Indian Ocean tropospheric aerosol, *J. Geophys. Res.*, in press, 2001.
- Marshak, A., A. Davis, W. Wiscombe, W. Ridgway, and R. Cahalan, Biases in shortwave column absorption in the presence of fractal clouds, *J. Clim.*, **11**, 431–446, 1998.
- Meywerk, J., and V. Ramanathan, Observations of the spectral clear-sky aerosol forcing over the tropical Indian Ocean, *J. Geophys. Res.*, **24**, 24,359–24,370, 1999.
- Novakov, T., D. A. Hegg, and P. V. Hobbs, Airborne measurements of carbonaceous aerosols on the east coast of the United States, *J. Geophys. Res.*, **102**, 30,023–30,030, 1997.
- Oberhuber, J. M., An atlas based on the ‘codes’ data set: The budgets of heat, buoyancy and turbulent kinetic energy at the surface of the global ocean, *Max Planck Inst. Meteorol. Rep. 15*, Max Planck Inst. for Meteorol., Hamburg, Germany, 1988.
- Pilinis, C., S. N. Pandis, and J. H. Seinfeld, Sensitivity of direct climate forcing by atmospheric aerosols to aerosol size and composition, *J. Geophys. Res.*, **100**, 18,739–18,754, 1995.
- Podgorny, I. A., A. M. Vogelmann, and V. Ramanathan, Effects of cloud shape and water vapor distribution on solar absorption in the near infrared, *Geophys. Res. Lett.*, **25**, 1899–1902, 1998.
- Podgorny, I. A., W. C. Conant, V. Ramanathan, and S. K. Satheesh, Aerosol modulation of atmospheric and solar heating over the tropical Indian Ocean, *Tellus, Ser. B*, **52**, 947–958, 2000.
- Ramanathan, V., B. Subasilar, G. J. Zhang, W. Conant, R. D. Cess, J. T. Kiehl, H. Grassl, and L. Shi, Warm pool heat budget and shortwave cloud forcing: A missing physics?, *Science*, **267**, 499–503, 1995.
- Ramanathan, V., et al., Indian Ocean Experiment (INDOEX), a multi-agency proposal for a field experiment in the Indian Ocean, C4, Scripps Inst. of Oceanogr., UCSD, La Jolla, Calif., 1996.
- Ramanathan, V., et al., Indian Ocean Experiment: An integrated analysis of the climate forcing and effects of the great Indo-Asian haze, *J. Geophys. Res.*, in press, 2001.
- Reid, J. S., P. V. Hobbs, C. Liousse, J. V. Martins, R. E. Weiss, and T. F. Eck, Comparisons of techniques for measuring shortwave absorption and black carbon content of aerosols from biomass burning in Brazil, *J. Geophys. Res.*, **103**, 32,031–32,040, 1998.
- Rossow, W. B., A. W. Walker, D. E. Beusichel, and M. D. Roiter, International Satellite Cloud Climatology Project (ISCCP) documentation of new cloud datasets, *WMO/TD-737*, 115 pp., World Meteorol. Organ., Geneva, Switzerland, 1996.
- Russell, P. B., P. V. Hobbs, and L. L. Stowe, Aerosol properties and radiative effects in the United States east coast haze plume: An overview of the Tropospheric Aerosol Radiative Forcing Observational Experiment (TARFOX), *J. Geophys. Res.*, **104**, 2213–2222, 1999.
- Satheesh, S. K., and V. Ramanathan, Observations of large difference in tropical aerosol forcing at the Earth’s surface and top of the atmosphere, *Nature*, **405**, 60–63, 2000.
- Satheesh, S. K., V. Ramanathan, X.-L. Jones, J. M. Lobert, I. A. Podgorny, J. M. Prospero, B. N. Holben, and N. G. Loeb, A model for the natural and anthropogenic aerosols over the tropical Indian Ocean derived from Indian Ocean Experiment data, *J. Geophys. Res.*, **104**, 27,421–27,440, 1999.
- Vogelmann, A. M., V. Ramanathan, and I. A. Podgorny, Scale dependence of solar heating rates in convective cloud systems with implications to General Circulation Models, *J. Clim.*, **14**, 1738–1752, 2001.

I. A. Podgorny and V. Ramanathan, Center for Atmospheric Sciences, Scripps Institution of Oceanography, University of California, San Diego, Mail Code 0221, 9500 Gilman Drive, La Jolla, CA 92093-0221, USA. (igor@fiji.ucsd.edu)

(Received May 16, 2000; revised March 26, 2001; accepted April 2, 2001.)

